

Review

Chalcopyrite Thin Film Materials for Photoelectrochemical Hydrogen Evolution from Water under Sunlight

Hiroyuki Kaneko, Tsutomu Minegishi and Kazunari Domen *

Department of Chemical System Engineering, The University of Tokyo, 7-3-1 Hongo, Bunkyo-ku, Tokyo 113-8656, Japan; E-Mails: h_kaneko@chemsys.t.u-tokyo.ac.jp (H.K.); tmine@chemsys.t.u-tokyo.ac.jp (T.M.)

* Author to whom correspondence should be addressed; E-Mail: domen@chemsys.t.u-tokyo.ac.jp; Tel.: +81-3-5841-1148; Fax: +81-3-5841-8838.

Academic Editor: Francesco Di Benedetto

Received: 30 May 2015 / Accepted: 14 July 2015 / Published: 17 July 2015

Abstract: Copper chalcopyrite is a promising candidate for a photocathode material for photoelectrochemical (PEC) water splitting because of its high half-cell solar-to-hydrogen conversion efficiency (HC-STH), relatively simple and low-cost preparation process, and chemical stability. This paper reviews recent advances in copper chalcopyrite photocathodes. The PEC properties of copper chalcopyrite photocathodes have improved fairly rapidly: HC-STH values of 0.25% and 8.5% in 2012 and 2015, respectively. On the other hand, the onset potential remains insufficient, owing to the shallow valence band maximum mainly consisting of Cu 3d orbitals. In order to improve the onset potential, we explored substituting Cu for Ag and investigate the PEC properties of silver gallium selenide (AGSe) thin film photocathodes for varying compositions, film growth atmospheres, and surfaces. The modified AGSe photocathodes showed a higher onset potential than copper chalcopyrite photocathodes. It was demonstrated that element substitution of copper chalcopyrite can help to achieve more efficient PEC water splitting.

Keywords: photoelectrochemical water splitting; hydrogen; photocathode; chalcopyrites; materials and thin film characterization

1. Introduction

Hydrogen is considered to be a promising alternative to conventional fossil fuels, such as petroleum, coal, and natural gas. Photoelectrochemical (PEC) water splitting is poised to become a viable method for producing hydrogen utilizing solar energy. The discovery of the Honda-Fujishima effect in 1972 has stimulated extensive research on PEC water splitting, and a large number of semiconducting materials have been investigated as photoelectrodes to achieve efficient PEC water splitting [1–4].

Photoexcited holes and electrons separated by the band bending at the semiconductor-electrolyte interface of semiconductor photoelectrodes can result in the oxidation and reduction of water, respectively. Generally, oxygen evolution reactions (OERs), and hydrogen evolution reactions (HERs) take place on the surfaces of n-type semiconductor electrodes, accompanied by upward band bending, and of p-type semiconductor electrodes, accompanied by downward band bending at the solid-liquid interfaces, respectively. Consequently, n-type and p-type semiconductor electrodes act as photoanodes and photocathodes, respectively. From the viewpoint of practical hydrogen production through PEC water splitting, the system should exhibit a large photocurrent without an external bias voltage and stable water splitting over the long term. Given a water oxidation potential of 1.23 VRHE and a reduction potential of 0 VRHE, in the case of driving water splitting reactions by combination of a photoanode and a photocathode, both photoelectrodes should show a large enough photocurrent at around 0.6 VRHE, and therefore, the onset potential of the photocathode (photoanode) should be more positive (negative) than 0.6 VRHE. Since the flat-band potential of a semiconductor electrode reflects the Fermi level of the semiconductor material [5], band edge engineering of the photoelectrode material combined with conductivity control is essential to achieving the desirable PEC properties for applications.

Various types of oxide- and (oxy)nitride-based n-type semiconductor materials, such as hematite [6–8], vanadate [9,10], the GaN:ZnO solid solution [11], nitrides [12,13], and oxynitrides [14,15] have been reported as photoanode materials. In the case of the photoanode, self-oxidation makes it difficult to utilize non-oxide materials. In contrast, the photocathode can be made of a non-oxide material, such as p-type Si [16–19], copper oxide [20,21], phosphides [22–25], and oxysulfides [26,27]. Most photocathodes showing a relatively high half-cell solar-to-hydrogen conversion efficiency (HC-STH) [28] have been composed of single-crystalline materials, as in the cases of Si, InP, and InGaP₂, owing to their low defect densities; however, these electrodes require time-consuming and costly processes to fabricate. Recently, it has been reported that copper chalcopyrite photocathodes in the polycrystalline state show relatively high HC-STH values that are comparable even to those of photocathodes consisting of the abovementioned single-crystalline materials. The main features of chalcopyrite materials are tunable band gaps from the visible light region to the infrared region, high optical absorption coefficients in the visible region, and relatively simple and low-cost preparation processes.

In the present review, we focus on chalcopyrite materials for hydrogen evolution by water reduction under visible light. Following a survey of chalcopyrite photocathodes, we discuss the improvement in onset potential achieved in these photocathodes by deepening the valence band maximum (VBM). We substitute Cu for Ag and determine the PEC properties of silver-gallium-selenide-based photocathodes. The effects of surface modification and hydrogen introduction during crystal growth on the PEC properties are also investigated.

2. Hydrogen Evolution from Water Using Copper Chalcocrite Photocathodes

I–III–VI₂ chalcocrites have been investigated as both photocatalysts and photocathodes. In the 2000s, it was reported that hydrogen evolution using AgInS₂ from an aqueous solution with sacrificial reagents [29] and that using solid solutions with ZnS and CuInS₂ showed relatively high photocatalytic activity [29–31]. Recently, Kato *et al.* reported photoelectrochemical and photocatalytic water splitting using the combination of a solid solution of CuGaS₂ and ZnS for hydrogen evolution and BiVO₄ for oxygen evolution [32].

Such chalcocrite-based semiconductors are also expected to be likely candidates for a photocathode owing to their p-type semiconductor properties, suitable conduction band minimum for hydrogen evolution through water reduction, and high optical absorption coefficient in the visible region ($2 \times 10^4 \text{ cm}^{-1}$ at 2.0 eV and $6 \times 10^4 \text{ cm}^{-1}$ at 2.6 eV for CuGaSe₂) [33]. We note that, from the 1970s on, CuGaSe₂, CuInSe₂, and Cu(In,Ga)Se₂ have been investigated for photoelectrochemical applications as well as solar cells [34–36].

After Valderrama *et al.* demonstrated HER using Cu(In,Ga)Se₂ in 2005 [37], various types of copper-based chalcocrite materials have been investigated as photocathodes for water splitting. Marsen *et al.* reported the usability of CuGaSe₂ as a photocathode [38]. Despite its small grain size of <100 nm, the photocathode showed a cathodic photocurrent of 16.6 mA/cm² under sunlight. Usability in the polycrystalline state can be another advantage of these materials, because most efficient photoelectrodes currently use single-crystalline materials, which are expensive and are prepared by time-consuming processes [39]. CuGaSe₂ has a relatively long absorption edge of 750 nm, and shows a relatively high incident-photon-to-current efficiency (IPCE) in the visible region, e.g., 63% at 640 nm under an applied potential of $-0.65 \text{ V}_{\text{SCE}}$ [40]. In these studies, acidic electrolytes such as 0.5 M H₂SO₄ were used and no surface modifications were explored. In 2010, Yokoyama *et al.* reported hydrogen evolution from water using surface-modified Cu(In,Ga)Se₂ photocathodes, *viz.*, Pt-modified Cu(In,Ga)Se₂ (Pt/CIGS), and Pt- and CdS-modified Cu(In,Ga)Se₂ (Pt/CdS/CIGS), in an aqueous solution of 0.1 M Na₂SO₄ with the pH adjusted to 9.5 by the addition of NaOH [41]. In that study, the Pt deposited on the photocathodes as nanoparticles served as a HER catalyst. Moreover, the Pt/CdS/CIGS electrode generated a three-times-larger photocurrent with a 0.3 V higher onset potential than Pt/CIGS. The CdS layer enhanced the charge separation through forming a p-n junction with the CIGS layer at the solid-liquid interface, resulting in the larger photocurrent and higher onset potential.

In 2013, Moriya *et al.* demonstrated long-term hydrogen evolution from water under visible light using a CdS- and Pt-modified CuGaSe₂ (Pt/CdS/CuGaSe₂) photocathode [42]. The Pt/CdS/CuGaSe₂ photocathode showed a larger photocurrent than Pt-modified CuGaSe₂ (Figure 1) with an HC-STH of 0.83% at the maximum and stable hydrogen production at 0 V_{RHE} for over 10 days (Figure 2). Photocathodes made of powders of copper gallium selenide (CGSe, Ga/Cu = 2) fabricated using the particle transfer method were also investigated and found to be applicable to the photocathode [43,44]. Such powder materials are preferable from the viewpoint of scalability as well as allowing a liquid-phase process to be employed. As with the report by Yokoyama *et al.* [41], the CGSe photocathode with a CdS layer (Pt/CdS/CGSe) showed a larger photocurrent and higher onset potential than that without CdS (Pt/CGSe). To reveal the details of the function of the CdS layer, the band alignment at the solid-liquid interface was calculated using Poisson's equation. The calculation showed that insertion of a CdS layer

with a thickness of several tens of nanometers leads to a thicker depletion layer, owing to the formation of a p-n junction and appropriate pinned potentials of band edges of the outer CdS layer at the solid-liquid interface. Thus, charge separation is promoted to extract excited electrons to the surface without recombination. Moreover, the large VBM offset of 0.98 eV between CGSe and CdS also prevents the diffusion of holes to the electrode surface, resulting in a larger photocurrent with a higher onset potential for Pt/CdS/CGSe than for Pt/CGSe.

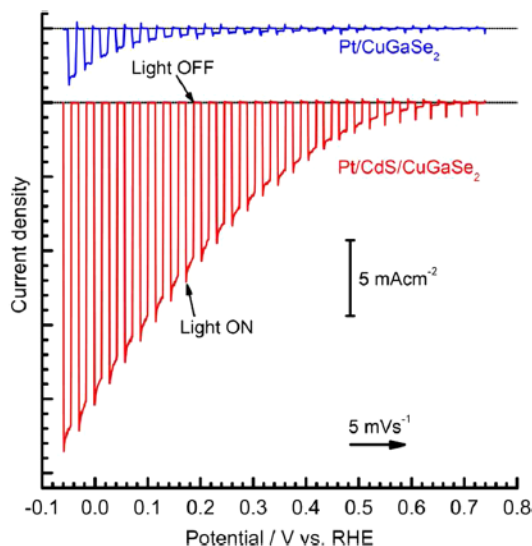


Figure 1. Current-potential curves for Pt/CuGaSe₂ and Pt/CdS/CuGaSe₂ electrodes [0.1 M Na₂SO₄(aq), pH 9, 300 W Xe lamp]. Reprinted with permission from Reference [42] (Copyright American Chemical Society 2013).

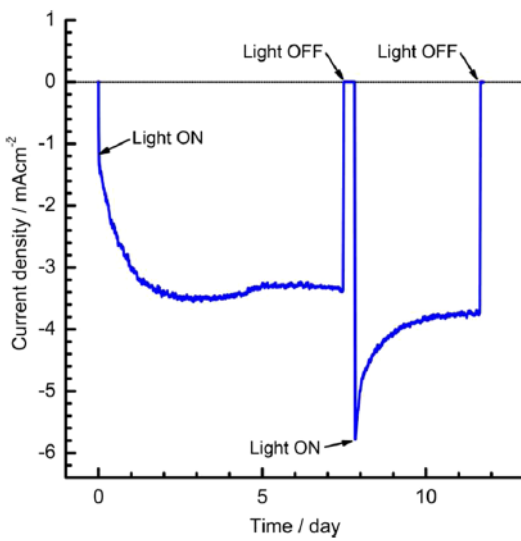


Figure 2. Current-time curve for a Pt/CdS/CuGaSe₂ electrode [0.05 M Na₂HPO₄(aq) + 0.05 M NaH₂PO₄(aq), pH 7, 150 W Xe lamp, 0 V_{RHE}]. Reprinted with permission from Reference [42] (Copyright American Chemical Society 2013).

Zhang *et al.* investigated the PEC properties of Pt- and CdS-modified Ag_xCu_{1-x}GaSe₂ (Pt/CdS/Ag_xCu_{1-x}GaSe₂) photocathodes by partial substitution of Cu with Ag [45], which they found

resulted in a higher HC-STH (1.22% at 0.3 V_{RHE}) than that of Pt/CdS/CuGaSe₂. The small grain size of conventional CuGaSe₂ limited the photocurrent; the partial substitution with Ag led to a significantly larger grain size thanks to the relatively low melting point of AgGaSe₂ (Figure 3). It was found that the optimum ratio of Ag to Cu for the HC-STH is Ag/(Ag + Cu) = 5.9%. For further increases in photocurrent and onset potential, the effects of the multilayer structure were investigated [46]. Inserting a CuGa₃Se₅ layer between CdS and Ag_xCu_{1-x}GaSe₂ (Pt/CdS/CuGa₃Se₅/Ag_xCu_{1-x}GaSe₂) increased the onset potential by 0.14 V. The thickness of the depletion layer was calculated to be 234 nm for both Pt/CdS/CuGa₃Se₅/Ag_xCu_{1-x}GaSe₂ and Pt/CdS/Ag_xCu_{1-x}GaSe₂ at 0.6 V_{RHE}. Thus, the increases in photocurrent and onset potential are attributable to a lower rate of carrier recombination. Since the CuGa₃Se₅/Ag_xCu_{1-x}GaSe₂ interface is prepared *in situ*, resulting in the formation of a high-quality CuGa₃Se₅/Ag_xCu_{1-x}GaSe₂ interface, recombination at the interface is significantly suppressed. Moreover, calculations of the band alignment at the solid-liquid interface of CdS/CuGa₃Se₅/Ag_xCu_{1-x}GaSe₂ indicated that the band offsets of conduction band minimum (CBM) and VBM between CdS and Ag_xCu_{1-x}GaSe₂ with a stepped-down alignment prevent photoexcited holes from diffusing into the defective CdS/CuGa₃Se₅ interface, resulting in a higher onset potential and photocurrent value than Pt/CdS/Ag_xCu_{1-x}GaSe₂. It should be noted that the Pt/CdS/CuGa₃Se₅/Ag_xCu_{1-x}GaSe₂ photocathode produced hydrogen stably for over 19 days.

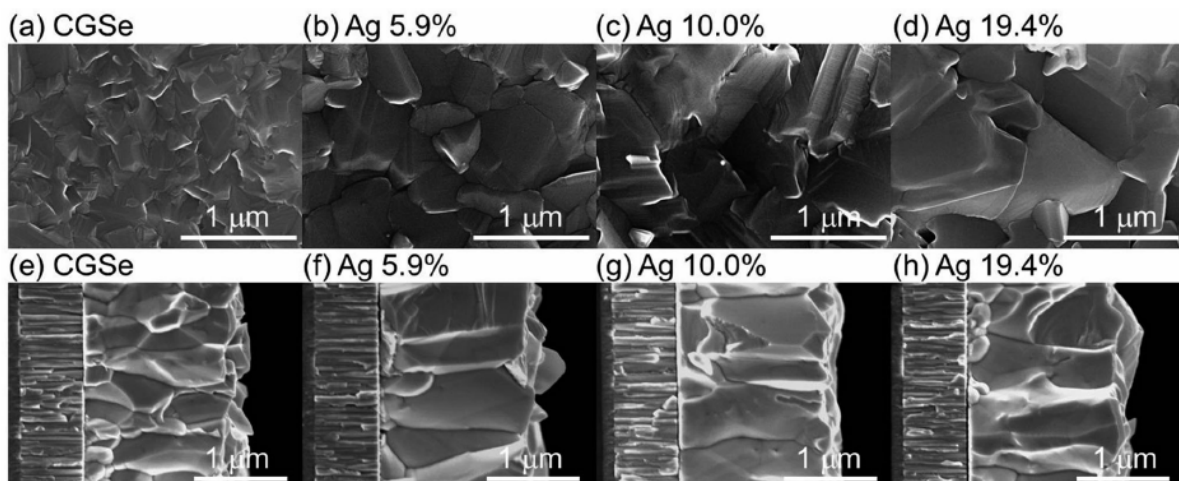


Figure 3. Top and cross-sectional views of CuGaSe₂ (**a**), (**e**), and Ag_xCu_{1-x}GaSe₂ films with $x = 5.9\%$ (**b**), (**f**), 10.0% (**c**), (**g**), 19.4% (**d**), (**h**). Reproduced from Reference [45] with permission (Copyright The Royal Society of Chemistry 2014).

A large leap in maximum photocurrent and HC-STH was achieved using a surface-modified CIGS-based photocathode with thin conductor layers employing a neutral phosphate buffer solution as an electrolyte [47]. This suggested that a conductor layer such as titanium and molybdenum prevents the formation of a Schottky barrier between Pt and CdS. Furthermore, because the conductor layer is electron-rich, it acts as a mediator, ensuring the smooth transfer of electrons from CdS to active sites (Figure 4). By contrast, in the absence of a conductor layer, minority carriers generated in the CIGS layer need to reach the active sites directly. Consequently, the Pt-, Mo-, Ti-, and CdS-modified CIGS (Pt/Mo/Ti/CdS/CIGS) photocathode showed a maximum photocurrent of 30 mA/cm² and a maximum

HC-STH of 8.5%, which are the highest values reported to date for a photocathode based on polycrystalline materials (Figure 5).

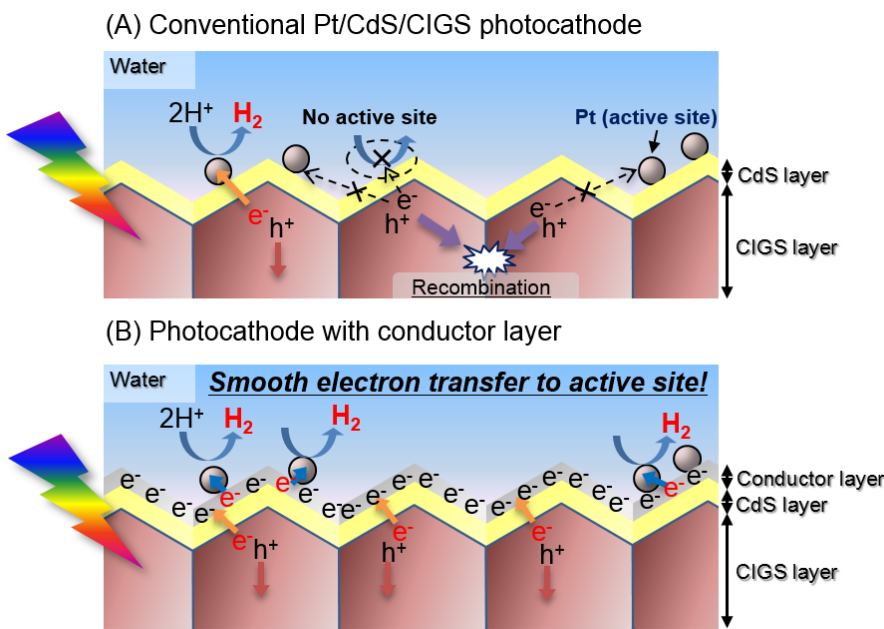


Figure 4. Proposed mechanisms for hydrogen evolution on the surfaces of CIGS photocathodes with and without a conductor layer. Adapted from Reference [47] with permission (Copyright The Royal Society of Chemistry 2015).

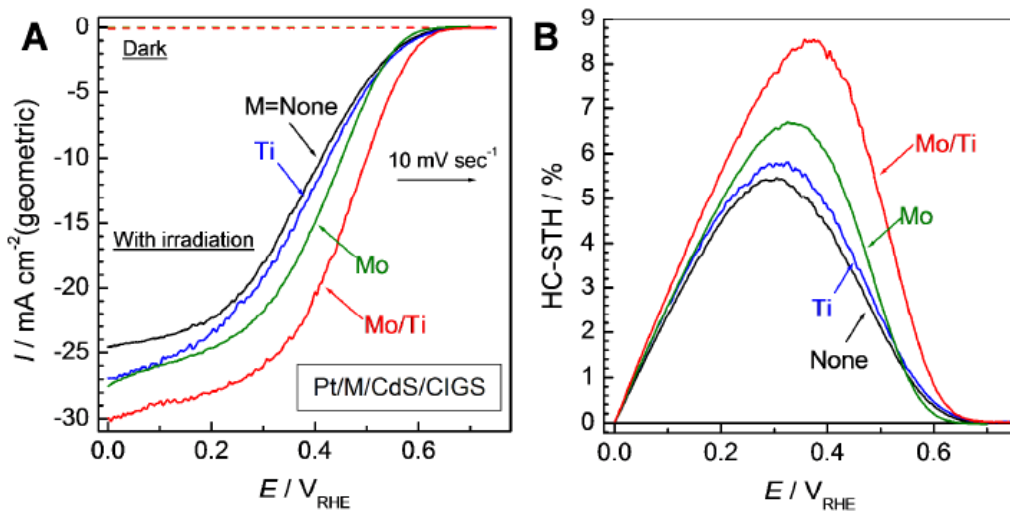


Figure 5. (A) Current-potential curves and (B) corresponding HC-STH values for $\text{Pt}/\text{M}/\text{Cu}(\text{In},\text{Ga})\text{Se}_2$ electrodes ($\text{M} = \text{none, Ti, Mo, Mo/Ti}$) [$0.5 \text{ M Na}_2\text{SO}_4(\text{aq}) + 0.25 \text{ M Na}_2\text{HPO}_4(\text{aq}) + 0.05 \text{ M NaH}_2\text{PO}_4(\text{aq})$, pH 6.8, AM1.5G]. Reproduced from Reference [47] with permission (Copyright The Royal Society of Chemistry 2015).

From the viewpoint of solar energy harvesting, the scalability of the photoelectrode fabrication method is an important factor. The photocathodes described above are prepared by vacuum evaporation methods, which are not very scalable. Some photocathodes based on copper chalcopyrites can be

prepared by scalable methods. Ikeda *et al.* have reported hydrogen evolution from water using Pt- and CdS-modified CuInS₂ (CIS) photocathodes. The CIS thin films were prepared by a combination of electrodeposition and sulfurization, which is scalable and cost-effective [48]. Pt- and CdS-modified CIS (Pt/CdS/CIS) photocathodes showed IPCEs above 20% at wavelengths ranging from 500 nm to 750 nm at -0.37 V_{RHE}. These results indicate that CIS prepared by a liquid-based process can show a photocurrent comparable to that for other copper-chalcopyrite-based photocathodes prepared by vacuum processing. Recently, Gunawan *et al.* reported that In₂S₃ is preferable to CdS as a surface modifier for CIS photocathodes. A Pt- and In₂S₃-modified CIS (Pt/In₂S₃/CIS) photocathode showed a photocurrent of 15 mA/cm² at 0 V_{RHE} under AM1.5G irradiation. One of the most important problems with CIS-based photocathodes is the instability of the photocurrent. Zhao *et al.* achieved stabilization of the photocurrent and hydrogen evolution for over an hour. The deposition of an additional TiO₂ layer with an appropriate thickness on CdS-modified CIS, followed by Pt deposition, served as a protective layer, enabling stable PEC hydrogen evolution from water with a faradaic efficiency of ~90% [49].

In summary, the performance of photocathodes based on copper chalcopyrite materials has improved rapidly: the maximum HC-STH increased from 0.25% to 8.5% between 2012 and 2015 (Table 1). Thus, chalcopyrite photocathodes are promising materials for the PEC hydrogen production system.

It also should be noted that *p*-type Cu₂ZnSnS₄, which has a kesterite structure, has been investigated as a photocathode, and shows photocurrent values comparable to those of chalcopyrite materials [50–52]. This material is attractive in that it is made of Earth-abundant and low-toxicity elements.

3. Band Structure Modulation by Composition Control

However, copper chalcogenide photocathodes show a maximum HC-STH at potentials more negative than 0.4 V_{RHE}. Considering combination with photoanodes without external bias voltage, the photocathodes should show a sufficient photocurrent above 0.6 V_{RHE}. Because copper chalcopyrites, such as CuGaSe₂, CIS, and CIGS, have a relatively shallow VBM, mainly because of the Cu 3d orbitals [53], their onset potential is more negative than the desired potential. Therefore, the photocurrent at positive potentials is limited. Increasing their onset potentials requires deepening their VBM by band engineering.

As mentioned above, the VBM of copper chalcopyrites involves Cu 3d orbitals. Thus, two strategies can be employed to obtain a deeper VBM: decreasing the amount of Cu and/or substituting Cu for another element, such as Ag. In 2012, Kim *et al.* reported that a CuGa₃Se₅-based photocathode modified with Pt (Pt/CuGa₃Se₅) showed a higher onset potential than a Pt-modified CuGaSe₂ photocathode [54]. The higher onset potential of the cathodic photocurrent is due to the deeper VBM potential of CuGa₃Se₅ against CuGaSe₂. We note that CuGa₃Se₅ contains Cu vacancies and Gac_u antisites, decreasing the influence of Cu 3d orbitals on the VBM potential.

Given that the potentials of Ag 4d orbitals are much deeper than those of Cu 3d orbitals [55], another way to deepen the VBM is to substitute Cu with Ag. Silver chalcopyrites have been investigated for PV applications [56,57]. However, there are no reports on its photocathodes. In the next chapter, PEC properties of gallium selenide and silver gallium selenide are discussed, with an eye toward more positive onset potentials compared to those of copper chalcopyrite photocathodes.

Table 1. Reported PEC properties of copper chalcopyrite photocathodes.

Photocathode [Electrolyte]	Published Year	Photocurrent Value at 0 V _{RHE}	IPCE at 0 V _{RHE}	Maximum HC-STH	Stability at 0 V _{RHE}	Ref.
Pt/CdS/CIGS [0.1 M Na ₂ SO ₄ pH 9.5]	2010	12 mA cm ⁻² under Xe lamp	59% at 600 nm (at -0.24 V _{RHE})	N.A.	Unstable	[41]
Pt/CdS/CIS [0.1 M Na ₂ SO ₄ pH 13]	2011	6 mA cm ⁻² under Xe lamp	>20% at 500–750 nm (at -0.37 V _{RHE} in pH 4)	N.A.	N.A.	[48]
Pt/CuGa ₃ Se ₅ [0.1 M Na ₂ SO ₄ pH 9.5]	2012	4.95 mA cm ⁻² under AM1.5G	15% at 600 nm	0.35% at 0.17 V _{RHE}	N.A.	[58]
Pt/ZnS/CuGa ₃ Se ₅ [0.1 M Na ₂ SO ₄ pH 9.5]	2012	4.35 mA cm ⁻² under AM1.5G	25.4% at 520 nm	0.25% at 0.1 V _{RHE}	25 h (at 0.1 V _{RHE})	[54]
Pt/CdS/CuGaSe ₂ [0.1 M Na ₂ SO ₄ pH 9]	2013	7.5 mA cm ⁻² under AM1.5G	45% at 520 nm	0.83% at 0.2 V _{RHE}	>10 days	[42]
Pt/CdS/CGSe (powder, Ga/Cu = 2) [0.1 M Na ₂ SO ₄ pH 9.5]	2014	2.4 mA cm ⁻² under AM1.5D	N.A.	N.A.	16 h (at 0.1 V _{RHE})	[43]
Pt/CdS/Ag _x Cu _{1-x} GaSe ₂ (x = 5.9%) [0.1 M Na ₂ SO ₄ pH 9.5]	2014	8.1 mA cm ⁻² under AM1.5G	54% at 550 nm	1.22% at 0.3 V _{RHE}	55 h	[45]
Pt/In ₂ S ₃ /CIS [0.1 M Na ₂ SO ₄ pH 9]	2014	15 mA cm ⁻² under AM1.5G	37%–41% at 520–700 nm	1.97% at 0.28 V _{RHE}	N.A.	[59]
Pt/TiO ₂ /CdS/CIS [0.1 M Na ₂ HPO ₄ pH 10]	2014	13.0 mA cm ⁻² under AM1.5G	62% at 500–700 nm	1.82% at 0.25 V _{RHE}	1 h	[49]
Pt/CdS/CuGa ₃ Se ₅ / Ag _x Cu _{1-x} GaSe ₂ (x = 5.9%) [0.1 M Na ₂ HPO ₄ pH 10]	2015	8.79 mA cm ⁻² under AM1.5G	>57% at 520–600 nm	1.81% at 0.36 V _{RHE}	20 days	[46]
Pt/Mo/Ti/Cu(In,Ga)Se ₂ [0.5 M Na ₂ SO ₄ + 0.25 M Na ₂ HPO ₄ + 0.25 M NaH ₂ PO ₄ pH 6.8]	2015	30 mA cm ⁻² under AM1.5G	N.A.	8.5% at 0.38 V _{RHE}	10 days (with a decrease on a daily basis)	[47]

4. PEC Properties of AGSe Photocathodes

4.1. Experimental Methods

Gallium selenide and AGSe thin films with a thickness of ~1 μm were prepared by co-evaporation in a vacuum chamber. Mo-coated soda-lime glass (5 mm × 10 mm), prepared by RF magnetron sputtering deposition of a 50-nm-thick Ti layer to improve adhesivity, followed by a 400- to 500-nm-thick Mo layer, was used as a substrate. Elemental Ag, Ga, and Se with purities of 5N, 6N, and 6N, respectively, were heated in effusion cells and evaporated. The deposition rates of Ga and Se were kept at 0.06 and 0.5–1.0 nm/s, respectively, while that of Ag was varied between 0 and 0.05 nm/s, according to the required Ag/Ga ratio. The base pressure of the deposition chamber was 10⁻⁶ Pa.

To facilitate charge separation, CdS layers were deposited on prepared thin films by chemical bath deposition (CBD). The CBD solution contained 14 wt% ammonia (Wako), 25 mM of Cd(CH₃COO)₂

(Kanto, 98.0%), and 0.375 M of $\text{SC}(\text{NH}_2)_2$ (Kanto, 98.0%). After 1 min of CdS deposition, the samples were annealed in air at 573 K for 1 h.

These samples were analyzed using X-ray diffraction (XRD) (RINT-Ultima3, Rigaku, Tokyo, Japan), photoelectron spectroscopy in air (PESA) (AC-3, Riken Keiki, Tokyo, Japan), and scanning electron microscopy (SEM) (S-4700, Hitachi, Tokyo, Japan).

The typical three-electrode setup was used to characterize the PEC properties. A Pt wire and Ag/AgCl in saturated aqueous KCl solution were used as the counter and reference electrodes, respectively. The PEC measurements were performed under an Ar atmosphere using an aqueous solution containing 0.1 M Na_2SO_4 (pH adjusted to 9 by NaOH addition) as the electrolyte. The potentials obtained from each measurement were converted into values against a reversible hydrogen electrode (RHE). 300 W Xe lamp equipped with a cold mirror (CM-1, Optoline, Tokyo, Japan) and cutoff filter (L42, Hoya, Tokyo, Japan) was employed as the light source. The applied potential was swept in the positive direction at $10 \text{ mV}\cdot\text{s}^{-1}$ under intermittent irradiation of the Xe lamp from $-0.2 \text{ V}_{\text{RHE}}$ to the potential at which a cathodic photocurrent vanishes. To estimate the Faradaic efficiency of hydrogen generation, the gaseous products were analyzed using micro-gas chromatography (GC, GC3000A, Inficon, Bad Ragaz, Switzerland) in an airtight three-electrode cell.

Pt particles were deposited on the prepared electrodes by photo-assisted electrodeposition as hydrogen evolution catalysts. The electrodes were exposed to the 300 W Xe lamp equipped with filters while immersed in a solution containing 10 μM H_2PtCl_6 (Kanto, 98.5%), 10 μM NaOH (Wako, from 0.1 M solution), and 0.1 M Na_2SO_4 at a potential of -0.8 to $-0.6 \text{ V}_{\text{Ag/AgCl}}$ for 1–3 h.

4.2. Results and Discussion

4.2.1. PEC Properties of Gallium Selenide and AGSe Photocathodes

The XRD patterns for the prepared gallium selenide and AGSe ($\text{Ag/Ga} = 2\%–77\%$) films (see Figure 6) indicate that the gallium selenide films consisted of a layered GaSe (ϵ - GaSe) phase, while the AGSe films consisted of ϵ - GaSe and α - Ga_2Se_3 phases, whose XRD peaks shifted to lower angles with the Ag/Ga ratio increase, owing to the gradual formation of the defective chalcopyrite phase. It should be noted that α - Ga_2Se_3 , defect-containing chalcopyrite, and the defect-free chalcopyrite phase all have a kind of diamond structure. The only structural difference between these phases has to do with the absence/presence of vacancies and elemental substitutions. The XRD peaks for ϵ - GaSe did not show a clear shift in diffraction angle, which indicates that Ag was mainly incorporated into the α - Ga_2Se_3 phase. We note that the AgGaSe_2 phase was found in the pattern for AGSe with an Ag/Ga ratio of 77%.

The current-potential curves for Pt-loaded AGSe (Pt/AGSe) electrodes are shown in Figure 7. All electrodes exhibited a clear photo-response, and AGSe with an Ag/Ga ratio below 9% showed larger cathodic photocurrents with relatively high onset potentials of greater than $0.4 \text{ V}_{\text{RHE}}$. The anodic photo-response detected in the case of $>2\%$ Ag/Ga at potentials above the onset potentials indicates that the prepared films contained *n*-type sections that limited the onset potential of the electrodes. This suggests that Ag-poor compositions are better at enhancing the *p*-type character of the prepared AGSe films. The Ag-free electrode showed the largest cathodic photocurrent and the highest onset potential of $0.5 \text{ V}_{\text{RHE}}$. However, a clear decrease in cathodic photocurrent was observed in the second potential

sweep, as seen in Figure 7. In contrast, AGSe with a Ag/Ga ratio of 2% did not show a clear decrease in the second sweep. Moreover, the AGSe photocathode worked stably for over 12 h (Figure S1). The XRD results indicate that the Ag in AGSe plays an important role in preventing photo-reduction of the photocathode through the formation of the defect-containing chalcopyrite phase.

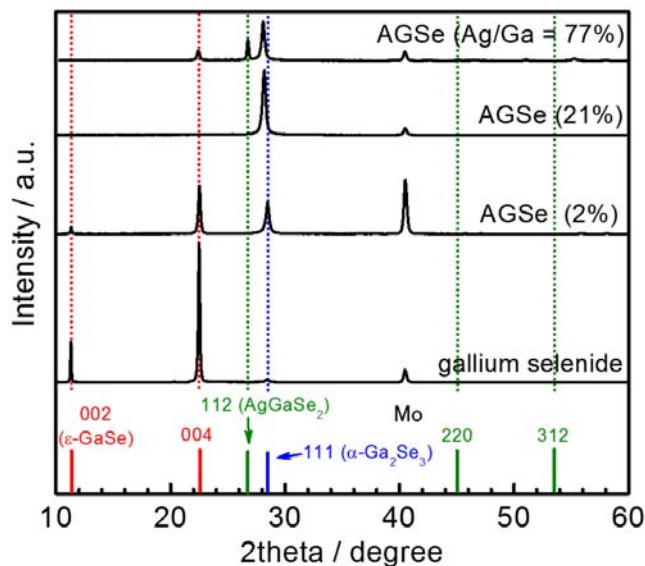


Figure 6. XRD patterns for gallium selenide and AGSe films prepared with various Ag/Ga ratios. Reference peak positions are shown. ICSD numbers of ϵ -GaSe, AgGaSe₂, and α -Ga₂Se₃ are #2002, #52570, and #35028, respectively.

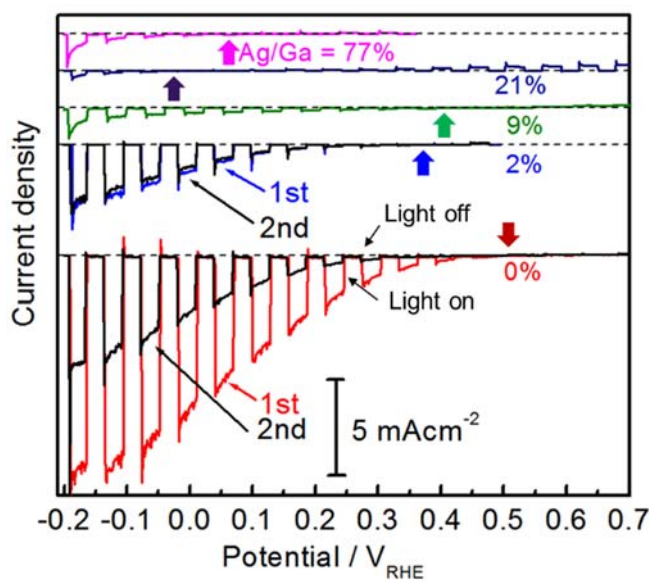


Figure 7. Current-potential curves for Pt/AGSe electrodes with various Ag/Ga ratios. A 0.1 M aqueous Na₂SO₄ solution (adjusted to pH 9 by NaOH addition) was employed as the electrolyte. Onsets of cathodic photocurrents are pointed out by arrows.

Figure 8 shows plane-view and cross-sectional SEM images of gallium selenide and AGSe ($\text{Ag}/\text{Ga} = 2\%$). These images indicate that a very small amount of Ag causes a significant variation in the film structure. As shown in Figure 8A, the gallium selenide film has a smooth surface with triquetrous facets and bead-like spheres. The cross-sectional view in Figure 8C reveals that the gallium selenide film is composed of parallel-lying flakes. The structure of the gallium selenide film is very similar to that reported by Chang *et al.* [60]. On the other hand, the cross-sectional SEM image in Figure 8D verifies that the AGSe ($\text{Ag}/\text{Ga} = 2\%$) film has a dense structure. This difference in film structure seems to be consistent with the XRD patterns shown in Figure 6, as the ϵ -GaSe film consists of a layered compound, while AGSe consists of a layered compound and defect-containing chalcopyrite.

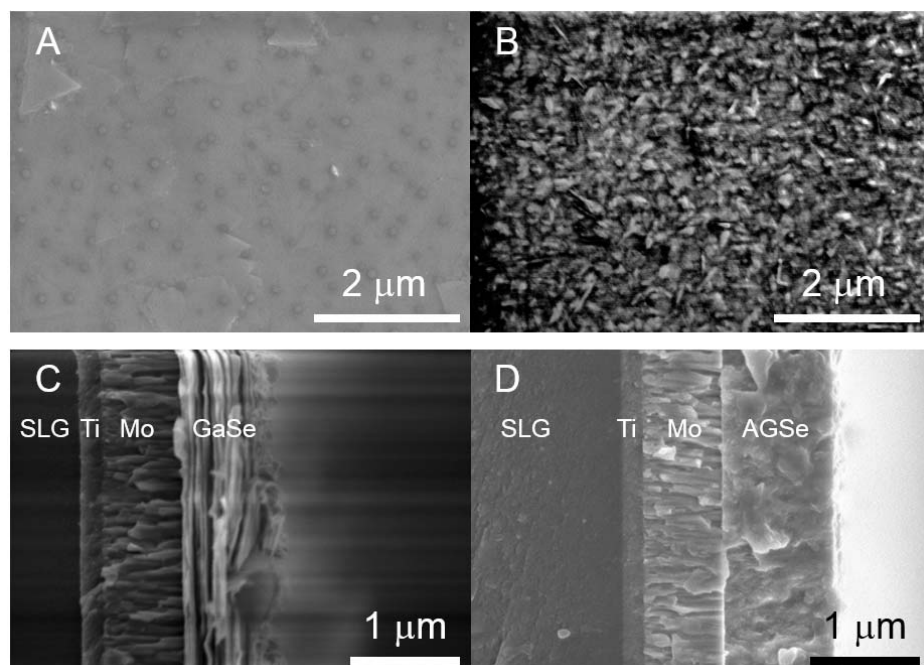


Figure 8. SEM images of a GaSe film (**A,C**) and AGSe ($\text{Ag}/\text{Ga} = 2\%$) film (**B,D**): plane (**A,B**) and cross-section (**C,D**). An ultrathin CdS layer (not detectable in these images) is deposited on the films for cross-sectional imaging.

To determine the VBM potential of gallium selenide and AGSe, PESA measurements were conducted. Interestingly, as shown in Figure 9, gallium selenide and AGSe ($\text{Ag}/\text{Ga} = 2\%$) showed VBM potentials deeper than $1.23 \text{ V}_{\text{NHE}}$. It is most likely that the phase transition, as shown in XRD pattern, contributes to the deeper VBM of AGSe ($\text{Ag}/\text{Ga} = 2\%$) than that of ϵ -GaSe. This indicates that gallium selenide and AGSe are very attractive materials because of the possibility of obtaining a high onset potential of $> 1.23 \text{ V}_{\text{RHE}}$. The difference in VBM potential between these materials is not fully consistent, with the difference in onset potential observed in the current-potential curves shown in Figure 7. We note that the onset potential is clearly lower than would be expected from the PESA results, especially the case of $\text{Ag}/\text{Ga} = 0\%$, because of the existence of local photoanodes in the prepared films, which is due to the tendency of ϵ -GaSe and AGSe to easily act as an *n*-type semiconductor, and because of the lack of proper surface modifications.

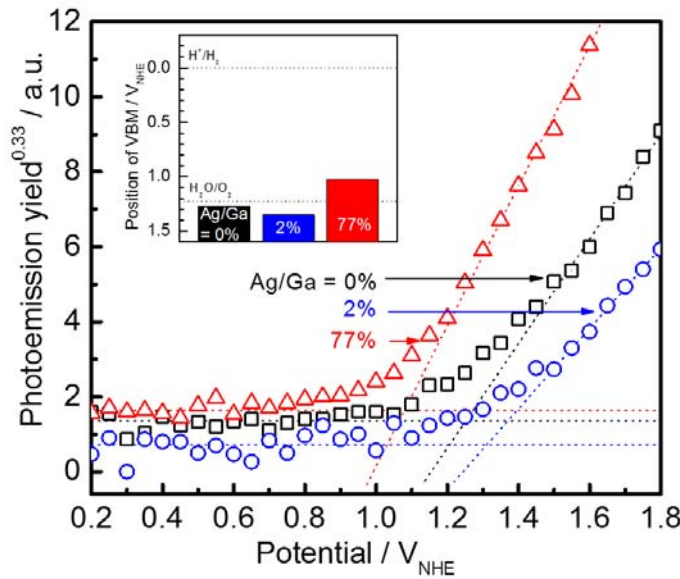


Figure 9. PESA spectra of the prepared AGSe with different Ag/Ga ratios and VBM positions.

4.2.2. Effects of CdS Modification and AGSe Film Preparation under Partial Pressure of Hydrogen

AGSe (Ag/Ga = 2%) showed the highest onset potential. However, its film structure was not desirable because it consisted of small grains. It has previously been reported that the introduction of hydrogen into the deposition chamber during the deposition of polycrystalline CuGa₃Se₅ films having a defect-containing chalcopyrite structure increases the grain size [54]. To demonstrate the potential of the AGSe electrode for water splitting, the effects of hydrogen introduction during AGSe film deposition on PEC properties were investigated.

Upon the introduction of hydrogen, the intensity ratio of ϵ -GaSe increased (Figure S2), and the surface became coarser as in the case of CuGa₃Se₅ (Figure S3) [54]. It is known that the introduction of hydrogen during deposition enhances the surface migration of adatoms, which leads to an increase in grain size [61,62]. Current-potential curves for Pt/AGSe prepared with and without hydrogen are shown in Figure 10. The introduction of hydrogen during deposition clearly more than doubled the cathodic photocurrent, while the increase in onset potential was negligible. The remarkable enhancement in cathodic photocurrent reflects the beneficial effects of hydrogen introduction into the deposition chamber during AGSe film preparation, although more significant increases in photocurrent have been reported for chalcopyrite materials. Unlike in the case of CuGa₃Se₅ [54], the XRD peaks did not become sharper, suggesting that the increase in photo-response was not due to an increase in the degree of crystallinity, but to a change in the crystal phase ratio. Interestingly, AGSe with the ϵ -GaSe phase is presumably a larger contributing factor to the increases in photocurrent and onset potential.

To facilitate the photocurrent, surface modification with CdS was conducted. Pt- and CdS-modified AGSe electrodes prepared with hydrogen introduction (Pt/CdS/AGSe(H₂)) showed a larger photocurrent and higher onset potential than those without CdS, as shown in Figure 10. In this case, CdS modification was very effective in increasing the onset potential and maximum photocurrent. We note that the surface modification with Pt and CdS was also effective to increase the photocurrent of AGSe photocathodes prepared without hydrogen introduction as shown in Figure S4. Indeed, Pt/CdS/AGSe(H₂) showed

clearly higher photocurrent ($7.5 \text{ mA} \cdot \text{cm}^{-2}$ at 0 V_{RHE}) and onset potential ($0.8 \text{ V}_{\text{RHE}}$) than Pt/AGSe(H_2) ($3.5 \text{ mA} \cdot \text{cm}^{-2}$ at 0 V_{RHE} ; and $0.4 \text{ V}_{\text{RHE}}$, respectively).

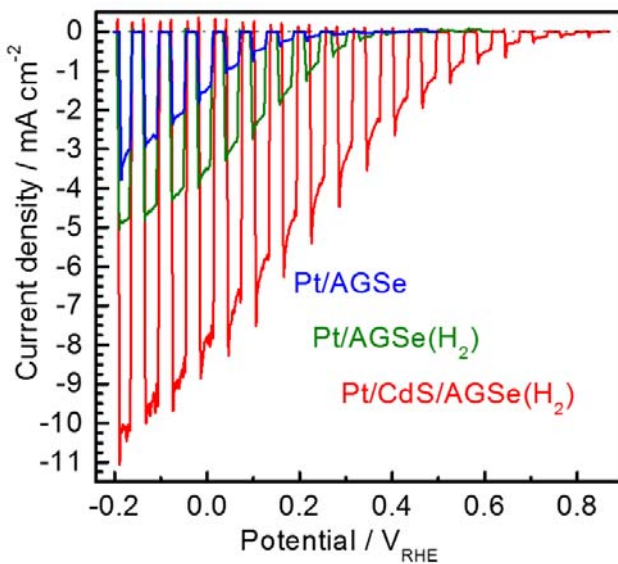


Figure 10. Current-potential curves for Pt/AGSe, Pt/AGSe(H_2), and Pt/CdS/AGSe(H_2) electrodes. A 0.1 M aqueous Na_2SO_4 solution (adjusted to pH 9 by NaOH addition) was employed as the electrolyte.

The band alignment for CdS/AGSe at a solid-liquid interface is schematized in Figure 11 on the basis of experimental results and reports. PESA results revealed that the VBM potential for AGSe is $+1.3 \text{ V}_{\text{NHE}}$, which is 0.4 V deeper than the reported value for CuGaSe_2 [42]. Given the VBM difference between CuGaSe_2 and CdS of 0.98 V and the VBM potential difference between AGSe and CuGaSe_2 , the VBM difference between AGSe and CdS is estimated to be 0.58 V. The pinned band edge potentials at solid-liquid interfaces can be estimated from the flat-band potential of CdS, reported to be $-0.1 \text{ V}_{\text{RHE}}$ at pH 9 [63].

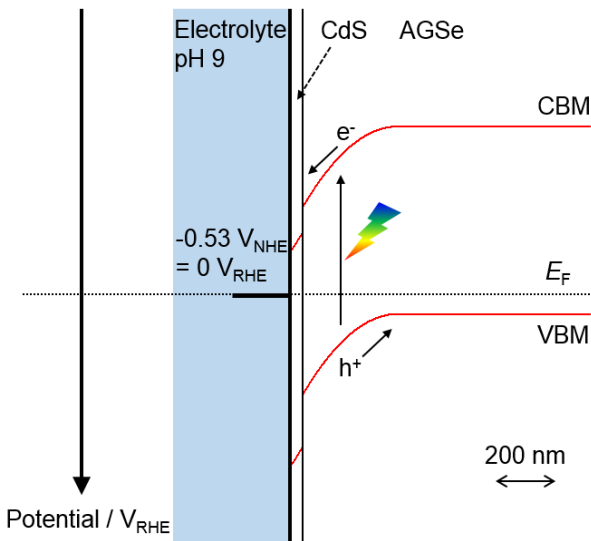


Figure 11. Schematic band alignment at a solid-electrolyte interface for the CdS/AGSe electrode.

The amount of evolved hydrogen gas was measured using micro-GC to confirm the contribution of the cathodic photocurrent to hydrogen evolution. The measurements revealed that the faradaic efficiency was 96%, as shown in Figure S5. This indicated that almost all of the photocurrent from the Pt/CdS/AGSe(H₂) photocathode contributed to HER.

The onset potential of the modified AGSe photocathode is more positive than that of copper chalcopyrite photocathodes. The deeper the VBM potential of the photocathode material, the more positive the onset potential, which is preferable. Controlling the VBM potential through compositional fine tuning, for example, by decreasing the amount of Cu, substituting Cu for another element, and/or alloying with II–VI compounds, can further improve the PEC properties [32,58].

5. Conclusions

Copper chalcopyrite materials are promising candidates for photocathode materials because of their relatively high HC-STH, usability in the polycrystalline state, and chemical stability. Recent reports show a rapid increase in the maximum HC-STHs of photocathodes based on copper chalcopyrite materials. However, the onset potentials of these copper chalcopyrite photocathodes have been limited by the shallowness of their VBMs due to the Cu 3d orbitals. To achieve efficient PEC water splitting with photoanodes, a higher onset potential is indispensable for copper chalcopyrite photocathodes.

Effective approaches to improving the onset potentials of copper chalcopyrite photocathodes, *i.e.*, to making them more positive, include deepening the VBM potential through compositional modifications, such as the substitution of Cu for Ag or decreasing the amount of Cu. To verify the effects of the substitution of Cu for Ag, the PEC properties of AGSe photocathodes were investigated in this study. A gallium-selenide-based photocathode showed a larger photocurrent than AGSe, even though gallium selenide cannot evolve hydrogen stably. SEM images and XRD patterns revealed that the surface morphology and crystal structure change significantly upon the addition of Ag, from parallel-lying flakes into triquetrous facets, which helps to prevent photocorrosion. PESA measurement results demonstrated that the VBM potential of AGSe is suitable for constructing a water splitting system with photoanodes, although the observed onset potential was more negative than expected from the PESA results, owing to the existence of local photoanodes in the AGSe film. Hydrogen introduction during AGSe deposition and surface modification with CdS increased both the photocurrent and onset potential of the AGSe photocathode, from 1.5 to 7.7 mA/cm² and from 0.4 to 0.8 V_{RHE}, respectively. The modified AGSe photocathode showed stoichiometric hydrogen evolution for about 1 h, and its onset potential was more positive than that for conventional photocathodes based on copper chalcopyrite materials. This work demonstrates that VBM engineering by, for example, the substitution of Cu for Ag, can contribute to the construction of a PEC overall water splitting system with photoanodes.

Acknowledgments

This work was supported by a Grant-in-Aid for Specially Promoted Research (#23000009) of the Japan Society for the Promotion of Science (JSPS), the Advanced Low Carbon Technology Research and Development Program (ALCA) of the Japan Science and Technology Agency (JST), the Global COE Program (Global Center of Excellence for Mechanical Systems Innovation) of the Ministry of Education, Culture, Sports, Science and Technology (MEXT) of Japan, and the international exchange

program of the A3 Foresight Program of JSPS. The author is supported by the Japan Society for the Promotion of Science through the Program for Leading Graduate Schools (MERIT).

Conflicts of Interest

The authors declare no conflict of interest.

References

1. Fujishima, A.; Honda, K. Electrochemical photolysis of water at a semiconductor electrode. *Nature* **1972**, *238*, 37–38.
2. Grätzel, M. Photoelectrochemical cells. *Nature* **2001**, *414*, 338–344.
3. Jacobsson, T.J.; Fjallstrom, V.; Sahlberg, M.; Edoff, M.; Edvinsson, T. A monolithic device for solar water splitting based on series interconnected thin film absorbers reaching over 10% solar-to-hydrogen efficiency. *Energy Environ. Sci.* **2013**, *6*, 3676–3683.
4. Yang, H. Bin; Miao, J.; Hung, S.; Huo, F.; Chen, H.M.; Liu, B.; Engineering, B.; Drive, N.; Road, R.; Science, M.; Avenue, N. Stable quantum dot photoelectrolysis cell for unassisted visible light solar. *ACS Nano* **2014**, *8*, 10403–10413.
5. Cendula, P.; Tilley, S.D.; Gimenez, S.; Bisquert, J.; Schmid, M.; Grätzel, M.; Schumacher, J.O. Calculation of the energy band diagram of a photoelectrochemical water splitting cell. *J. Phys. Chem. C* **2014**, *118*, 29599–29607.
6. Lin, Y.; Zhou, S.; Sheehan, S.W.; Wang, D. Nanonet-based hematite heteronanostructures for efficient solar water splitting. *J. Am. Chem. Soc.* **2011**, *133*, 2398–2401.
7. Zhang, M.; Lin, Y.; Mullen, T.J.; Lin, W.; Sun, L.; Yan, C.; Patten, T.E.; Wang, D.; Liu, G. Improving hematite's solar water splitting efficiency by incorporating rare-earth upconversion nanomaterials. *J. Phys. Chem. C* **2012**, 3188–3192.
8. Yang, X.; Liu, R.; Du, C.; Dai, P.; Zheng, Z.; Wang, D. Improving hematite-based photoelectrochemical water splitting with ultrathin TiO₂ by atomic layer deposition. *ACS Appl. Mater. Interfaces* **2014**, *6*, 12005–12011.
9. Jia, Q.; Iwashina, K.; Kudo, A. Facile fabrication of an efficient BiVO₄ thin film electrode for water splitting under visible light irradiation. *PNAS* **2012**, *109*, 11564–11569.
10. Kim, T.W.; Choi, K.-S. Nanoporous BiVO₄ photoanodes with dual-layer oxygen evolution catalysts for solar water splitting. *Science* **2014**, *343*, 990–994.
11. Zhong, M.; Ma, Y.; Oleynikov, P.; Domen, K.; Delaunay, J.-J. A conductive ZnO-ZnGaON nanowire-array-on-a-film photoanode for stable and efficient sunlight water splitting. *Energy Environ. Sci.* **2014**, *7*, 1693–1699.
12. Yokoyama, D.; Hashiguchi, H.; Maeda, K.; Minegishi, T.; Takata, T.; Abe, R.; Kubota, J.; Domen, K. Ta₃N₅ photoanodes for water splitting prepared by sputtering. *Thin Solid Films* **2011**, *519*, 2087–2092.
13. Li, Y.; Takata, T.; Cha, D.; Takanabe, K.; Minegishi, T.; Kubota, J.; Domen, K. Vertically aligned Ta₃N₅ nanorod arrays for solar-driven photoelectrochemical water splitting. *Adv. Mater.* **2013**, *25*, 125–131.

14. Urabe, H.; Hisatomi, T.; Minegishi, T.; Kubota, J.; Domen, K. Photoelectrochemical properties of SrNbO₂N photoanodes for water oxidation fabricated by the particle transfer method. *Faraday Discuss.* **2014**, *176*, 213–223.
15. Ueda, K.; Minegishi, T.; Clune, J.; Nakabayashi, M.; Hisatomi, T.; Nishiyama, H.; Katayama, M.; Shibata, N.; Kubota, J.; Yamada, T.; *et al.* Photoelectrochemical oxidation of water using BaTaO₂N photoanodes prepared by particle transfer method. *J. Am. Chem. Soc.* **2015**, *137*, 2227–2230.
16. Dominey, R.N.; Lewis, N.S.; Bruce, J.A.; Bookbinder, D.C.; Wrighton, M.S. Improvement of photoelectrochemical hydrogen generation by surface modification of *p*-type silicon semiconductor photocathodes. *J. Am. Chem. Soc.* **1982**, *104*, 467–482.
17. Fan, R.; Dong, W.; Fang, L.; Zheng, F.; Su, X.; Zou, S.; Huang, J.; Wang, X.; Shen, M. Stable and efficient multi-crystalline n⁺p silicon photocathode for H₂ production with pyramid-like surface nanostructure and thin Al₂O₃ protective layer. *Appl. Phys. Lett.* **2015**, *106*, doi:10.1063/1.4905511.
18. Bae, D.; Pedersen, T.; Seger, B.; Malizia, M.; Kuznetsov, A.; Hansen, O.; Chorkendorff, I.; Vesborg, P.C. K. Back-illuminated Si photocathode: a combined experimental and theoretical study for photocatalytic hydrogen evolution. *Energy Environ. Sci.* **2015**, *8*, 650–660.
19. Boettcher, S.W.; Warren, E.L.; Putnam, M.C.; Santori, E.A.; Turner-Evans, D.; Kelzenberg, M.D.; Walter, M.G.; McKone, J.R.; Brunschwig, B.S.; Atwater, H.A.; *et al.* Photoelectrochemical hydrogen evolution using Si microwire arrays. *J. Am. Chem. Soc.* **2011**, *133*, 1216–1219.
20. Morales-Guio, C.G.; Tilley, S.D.; Vrubel, H.; Grätzel, M.; Hu, X. Hydrogen evolution from a copper(I) oxide photocathode coated with an amorphous molybdenum sulphide catalyst. *Nat. Commun.* **2014**, *5*, doi:10.1038/ncomms4059.
21. Li, C.; Hisatomi, T.; Watanabe, O.; Nakabayashi, M.; Shibata, N.; Domen, K.; Delaunay, J.-J. Positive onset potential and stability of Cu₂O-based photocathodes in water splitting by atomic layer deposition of a Ga₂O₃ buffer layer. *Energy Environ. Sci.* **2015**, *8*, doi:10.1039/C5EE00250H.
22. Hu, S.; Shaner, M.R.; Beardslee, J.A.; Licherman, M.; Brunschwig, B.S.; Lewis, N.S. Amorphous TiO₂ coatings stabilize Si, GaAs, and GaP photoanodes for efficient water oxidation. *Science* **2014**, *344*, 1005–1009.
23. Lee, M.H.; Takei, K.; Zhang, J.; Kapadia, R.; Zheng, M.; Chen, Y.Z.; Nah, J.; Matthews, T.S.; Chueh, Y.L.; Ager, J.W.; Javey, A. p-Type InP nanopillar photocathodes for efficient solar-driven hydrogen production. *Angew. Chem. Int. Ed.* **2012**, *51*, 10760–10764.
24. Coridan, R.H.; Arpin, K.A.; Brunschwig, B.S.; Braun, P.V.; Lewis, N.S. Photoelectrochemical behavior of hierarchically structured Si/WO₃ core-shell tandem photoanodes. *Nano Lett.* **2014**, *14*, 2310–2317.
25. Liu, C.; Sun, J.; Tang, J.; Yang, P. Zn-doped p-type gallium phosphide nanowire photocathodes from a surfactant-free solution synthesis. *Nano Lett.* **2012**, *12*, 5407–5411.
26. Liu, J.; Hisatomi, T.; Ma, G.; Iwanaga, A.; Minegishi, T.; Moriya, Y.; Katayama, M.; Kubota, J.; Domen, K. Improving the photoelectrochemical activity of La₅Ti₂CuS₅O₇ for hydrogen evolution by particle transfer and doping. *Energy Environ. Sci.* **2014**, *7*, 2239–2242.
27. Ma, G.; Liu, J.; Hisatomi, T.; Minegishi, T.; Moriya, Y.; Iwase, M.; Nishiyama, H.; Katayama, M.; Yamada, T.; Domen, K. Site-selective photodeposition of Pt on a particulate Sc-La₅Ti₂CuS₅O₇ photocathode: Evidence for one-dimensional charge transfer. *Chem. Commun.* **2015**, *51*, 4302–4305.

28. Hisatomi, T.; Kubota, J.; Domen, K. Recent advances in semiconductors for photocatalytic and photoelectrochemical water splitting. *Chem. Soc. Rev.* **2014**, *43*, 7520–7535.
29. Tsuji, I.; Kato, H.; Kobayashi, H.; Kudo, A. Photocatalytic H₂ evolution reaction from aqueous solutions over band structure-controlled (AgIn)_xZn_{2(1-x)}S₂ solid solution photocatalysts with visible-light response and their surface nanostructures. *J. Am. Chem. Soc.* **2004**, *2*, 13406–13413.
30. Kudo, A.; Tsuji, I.; Kato, H. AgInZnS₉ solid solution photocatalyst for H₂ evolution from aqueous solutions under visible light irradiation. *Chem. Commun.* **2002**, *9*, 1958–1959.
31. Tsuji, I.; Kato, H.; Kudo, A. Visible-light-induced H₂ evolution from an aqueous solution containing sulfide and sulfite over a ZnS-CuInS₂-AgInS₂ solid-solution photocatalyst. *Angew. Chem. Int. Ed.* **2005**, *44*, 3565–3568.
32. Kato, T.; Hakari, Y.; Ikeda, S.; Jia, Q.; Iwase, A.; Kudo, A. Utilization of metal sulfide material of (CuGa)_{1-x}Zn_{2x}S₂ solid solution with visible light response in photocatalytic and photoelectrochemical solar water splitting systems. *J. Phys. Chem. Lett.* **2015**, 1042–1047.
33. Kindyak, V.V.; Kindyak, A.S.; Gremenok, V.F.; Bodnar, I.V.; Rud', Y.V.; Medvedkin, G.A. Optical properties of laser-evaporated CuGaSe₂ films near and above the fundamental absorption edge. *Thin Solid Films* **1994**, *250*, 33–36.
34. Kisilev, A.; Marcu, V.; Cahen, D.; Schock, H.W.; Noufi, R. Photoelectrochemical characterization of CuGaSe₂ and Cu(Ga, In)Se₂ films. *Sol. Cells* **1990**, *28*, 57–67.
35. Cahen, D.; Chen, Y.W. n-CuInSe₂ based photoelectrochemical cells: Improved, stable performance in aqueous polyiodide through rational surface and solution modifications. *Appl. Phys. Lett.* **1984**, *45*, 746–748.
36. Robbins, M.; Bachmann, K.J.; Lambrecht, V.G.; Thiel, F.A.; Thomson, J., Jr.; Vadimsky, R.G.; Menezes, S.; Heller, A.; Miller, B. CuInS₂ liquid junction solar cells. *J. Electrochem. Soc. Sol. State Sci. Technol.* **1978**, *125*, 831–832.
37. Valderrama, R.C.; Sebastian, P.J.; Enriquez, J.P.; Gamboa, S.A. Photoelectrochemical characterization of CIGS thin films for hydrogen production. *Sol. Energy Mater. Sol. Cells* **2005**, *88*, 145–155.
38. Marsen, B.; Cole, B.; Dorn, S.; Rocheleau, R.E.; Miller, E.L. Copper gallium diselenide photocathodes for solar photoelectrolysis. *Sol. Hydrog. Nanotechnol. II* **2007**, 6650, doi:10.1117/12.732737.
39. Wadia, C.; Alivisatos, A.P.; Kammen, D.M. Materials availability expands the opportunity for large-scale photovoltaics deployment. *Environ. Sci. Technol.* **2009**, *43*, 2072–2077.
40. Marsen, B.; Cole, B.; Miller, E.L. Photoelectrolysis of water using thin copper gallium diselenide electrodes. *Sol. Energy Mater. Sol. Cells* **2008**, *92*, 1054–1058.
41. Yokoyama, D.; Minegishi, T.; Maeda, K.; Katayama, M.; Kubota, J.; Yamada, A.; Konagai, M.; Domen, K. Photoelectrochemical water splitting using a Cu(In,Ga)Se₂ thin film. *Electrochim. commun.* **2010**, *12*, 851–853.
42. Moriya, M.; Minegishi, T.; Kumagai, H.; Katayama, M.; Kubota, J.; Domen, K. Stable hydrogen evolution from CdS modified CuGaSe₂ photoelectrode under visible light irradiation. *J. Am. Chem. Soc.* **2013**, *135*, 3733–3735.
43. Kumagai, H.; Minegishi, T.; Moriya, Y.; Kubota, J.; Domen, K. Photoelectrochemical hydrogen evolution from water using copper gallium selenide electrodes prepared by a particle transfer method. *J. Phys. Chem. C* **2014**, *118*, 16386–16392.

44. Minegishi, T.; Nishimura, N.; Kubota, J.; Domen, K. Photoelectrochemical properties of LaTiO₂N electrodes prepared by particle transfer for sunlight-driven water splitting. *Chem. Sci.* **2013**, *4*, 1120–1124.
45. Zhang, L.; Minegishi, T.; Kubota, J.; Domen, K. Hydrogen evolution from water using Ag_xCu_{1-x}GaSe₂ photocathodes under visible light. *Phys. Chem. Chem. Phys.* **2014**, *16*, 6167–6174.
46. Zhang, L.; Minegishi, T.; Nakabayashi, M.; Suzuki, Y.; Seki, K.; Shibata, N.; Kubota, J.; Domen, K. Durable hydrogen evolution from water driven by sunlight using (Ag,Cu)GaSe₂ photocathodes modified with CdS and CuGa₃Se₅. *Chem. Sci.* **2015**, *6*, 894–901.
47. Kumagai, H.; Minegishi, T.; Sato, N.; Yamada, T.; Kubota, J.; Domen, K. Efficient solar hydrogen production from neutral electrolytes using surface-modified Cu(In,Ga)Se₂ photocathodes. *J. Mater. Chem. A* **2015**, *3*, 8300–8307.
48. Ikeda, S.; Nakamura, T.; Lee, S.M.; Yagi, T.; Harada, T.; Minegishi, T.; Matsumura, M. Photoreduction of water by using modified CuInS₂ electrodes. *Chem. Sus. Chem.* **2011**, *4*, 262–268.
49. Zhao, J.; Minegishi, T.; Zhang, L.; Zhong, M.; Gunawan, R.; Nakabayashi, M.; Ma, G.; Hisatomi, T.; Katayama, M.; Ikeda, S.; *et al.* Enhancement of solar hydrogen evolution from water by surface modification with CdS and TiO₂ on porous CuInS₂ photocathodes prepared by an electrodeposition-sulfurization method. *Angew. Chemie Int. Ed.* **2014**, *53*, 11808–11812.
50. Ma, G.; Minegishi, T.; Yokoyama, D.; Kubota, J.; Domen, K. Photoelectrochemical hydrogen production on Cu₂ZnSnS₄/Mo-mesh thin-film electrodes prepared by electroplating. *Chem. Phys. Lett.* **2011**, *501*, 619–622.
51. Yokoyama, D.; Minegishi, T.; Jimbo, K.; Hisatomi, T.; Ma, G.; Katayama, M.; Kubota, J.; Katagiri, H.; Domen, K. H₂ evolution from water on modified Cu₂ZnSnS₄ photoelectrode under solar light. *Appl. Phys. Express* **2010**, *3*, doi:10.1143/APEX.3.101202.
52. Rovelli, L.; Tilley, S.D.; Sivula, K. Optimization and stabilization of electrodeposited Cu₂ZnSnS₄ photocathodes for solar water reduction. *ACS Appl. Mater. Interfaces* **2013**, *5*, 8018–8024.
53. Shay, J.L.; Tell, B.; Kasper, H.M.; Schiavone, L.M. p-d Hybridization of the valence bands of I-III-VI₂ compounds. *Phys. Rev. B* **1972**, *5*, 5003–5005.
54. Kim, J.; Minegishi, T.; Kobota, J.; Domen, K. Enhanced photoelectrochemical properties of CuGa₃Se₅ thin films for water splitting by the hydrogen mediated co-evaporation method. *Energy Environ. Sci.* **2012**, *5*, 6368–6374.
55. Hautier, G.; Ong, S.P.; Jain, A.; Moore, C.J.; Ceder, G. Accuracy of density functional theory in predicting formation energies of ternary oxides from binary oxides and its implication on phase stability. *Phys. Rev. B Condens. Matter Mater. Phys.* **2012**, *85*, doi:10.1103/PhysRevB.85.155208.
56. Simchi, H.; McCandless, B. An investigation of the surface properties of (Ag,Cu)(In,Ga)Se₂ thin films. *IEEE J. Photovoltaics* **2012**, *2*, 519–523.
57. Zhang, X.; Kobayashi, T.; Kurokawa, Y.; Miyajima, S.; Yamada, A. Deposition of Ag(In,Ga)Se₂ solar cells by a modified three-stage method using a low-temperature-deposited Ag-Se cap layer. *Jpn. J. Appl. Phys.* **2013**, *52*, 1–4.
58. Kim, J.; Minegishi, T.; Kobota, J.; Domen, K. Investigation of Cu-deficient copper gallium selenide thin film as a photocathode for photoelectrochemical water splitting. *Jpn. J. Appl. Phys.* **2012**, *51*, 1–6.

59. Gunawan; Septina, W.; Ikeda, S.; Harada, T.; Minegishi, T.; Domen, K.; Matsumura, M. Platinum and indium sulfide-modified CuInS₂ as efficient photocathodes for photoelectrochemical water splitting. *Chem. Commun.* **2014**, *50*, 8941–8943.
60. Chang, C.C.; Zeng, J.X.; Lan, S.M.; Uen, W.Y.; Liao, S.M.; Yang, T.N.; Ma, W.Y.; Chang, K.J. Fabrication of single-phase ϵ -GaSe films on Si(100) substrate by metal organic chemical vapor deposition. *Thin Solid Films* **2013**, *542*, 119–122.
61. Sano, M.; Miyamoto, K.; Kato, H.; Yao, T. Role of hydrogen in molecular beam epitaxy of ZnO. *Jpn. J. Appl. Phys.* **2004**, *95*, 5527–5531.
62. Chun, Y. Effect of atomic hydrogen in highly lattice-mismatched molecular beam epitaxy. *J. Cryst. Growth* **1995**, *150*, 497–502.
63. Watanabe, T.; Fujishima, A.; Honda, K. Potential variation at the semiconductor-electrolyte interface through a change in pH of the solution. *Chem. Lett.* **1974**, *3*, 897–900.

© 2015 by the authors; licensee MDPI, Basel, Switzerland. This article is an open access article distributed under the terms and conditions of the Creative Commons Attribution license (<http://creativecommons.org/licenses/by/4.0/>).